Materials & Design 233 (2023) 112262

Contents lists available at ScienceDirect

Materials & Design

journal homepage: www.elsevier.com/locate/matdes

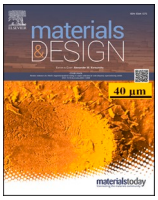

A biomimetic smart kirigami soft metamaterial with multimodal remote locomotion mechanisms

Benjamín Silva [a], Joseph Govan [b], Juan Cristóbal Zagal [c,d], Bruno Grossi [d,e], Alejandro Roldan [d,f], Alvaro S. Nunez [d,g], Daniel Acuña [d,g], Humberto Palza [a,d,h,*]

[a] Departamento de Ingeniería Química, Biotecnología y Materiales, Facultad de Ciencias Físicas y Matemáticas, Universidad de Chile, Chile
[b] Departamento de Ingeniería y suelos, Facultad de Ciencias Agronómicas, Universidad de Chile, Chile
[c] Departamento de Ingeniería Mecánica, Facultad de Ciencias Físicas y Matemáticas, Universidad de Chile, Chile
[d] ANID – Millenium Nucleus of Soft Smart Mechanical Metamaterials, Chile
[e] Centro de Investigación en Tecnologías para la Sociedad, Facultad de Ingeniería, Universidad del Desarrollo, Chile
[f] Departamento de ciencias naturales y tecnología Universidad de Aysén, Chile
[g] Departamento de Física, Facultad de Ciencias Físicas y Matemáticas, Universidad de Chile, Chile
[h] IMPACT, Center of Interventional Medicine for Precision and Advanced Cellular Therapy, Chile

ARTICLE INFO

Keywords:
Magneto-active materials
Soft robots
Mechanical metamaterials

ABSTRACT

Several efforts have been made to develop walking smart soft robots through different strategies such as the use of complex aligned magneto-active materials. Here, we show a simple approach for the design of a smart soft robot using an elastomer film with randomly distributed ferrimagnetic nanoparticles able to be remotely controlled by a magnetic field. The magneto-active robot has a rotating-square kirigami geometry resulting in a flexible smart auxetic metamaterial (i.e., a negative Poisson-ratio structure). Alongside the standard translational locomotion on a smooth-surface under a steady magnetic force, the auxetic kirigami structure mimics the crawling-locomotion of worms over a high-roughness surface under an oscillatory horizontal field, even climbing vertical-obstacles. A theoretical understanding for this new locomotion mechanism stresses the relevance of the kirigami metamaterial design and the ferrimagnetic response of the particles. The soft robot can also transport a payload having weights higher than the weight of the smart elastomeric film. The smart auxetic structure further presents a rolling locomotion by properly orienting the magnetic field, meaning multiple remote locomotion mechanisms.

1. Introduction

The design of soft robots uses the 'mechanical intelligence' resulting from the soft material properties and the corresponding structure/architecture to mimic the neuromechanical control system of animal locomotion through simple mechanisms [1]. A key component to mimic in soft body animals is the capacity to change and adapt in unsteady environments by controlling the contact time and force distribution on a surface, allowing for instance complex locomotion mechanisms [1]. Recently, mechanical metamaterials (i.e., structures with unusual properties arising from the designed architecture rather than from the intrinsic material property) has been highlighted for advanced soft robot design toward future intelligent machines [2]. These soft robots take advantage of the programmable actuation that results from the continues/monolithic metamaterial architectures to replace complex assembled structures or actuators [2]. For instance, coupled modules of buckling-driven elastomeric metamaterials actuated by a negative air-pressure mechanism can mimic the locomotion of caterpillars and other crawling organisms using a dynamic anchoring process [3]. In this context, kirigami cutting principles have been recently applied for the development of novel soft metamaterial actuators using mainly the geometry of the structure rather than the properties of the material [4–6]. The mechanical motions of kirigami patterns can produce unconventional material characteristics, such as highly stretchable smart surfaces able to transform flat sheets into a 3D-textured surfaces that mimics snake-skin and -crawling locomotion [4]. The locomotion highly

* Corresponding author at: Departamento de Ingeniería Química, Biotecnología y Materiales, Facultad de Ciencias Físicas y Matemáticas, Universidad de Chile, Chile; IMPACT, Center of Interventional Medicine for Precision and Advanced Cellular Therapy, Chile.
E-mail addresses: joseph.govan@uchile.cl (J. Govan), jczagal@ing.uchile.cl (J. Cristóbal Zagal), bruno.grossi@udd.cl (B. Grossi), alnunez@dfi.uchile.cl (A.S. Nunez), dacuna1@uc.cl (D. Acuña), hpalza@ing.uchile.cl (H. Palza).

https://doi.org/10.1016/j.matdes.2023.112262
Received 22 March 2023; Received in revised form 7 August 2023; Accepted 19 August 2023
Available online 21 August 2023

depended on the buckling instability occurring under uniaxial tension on the kirigami surface that results in a pattern with highly anisotropic frictional characteristics. The smart surface of this soft robot was pneumatically actuated using an internal fiber-reinforced elastomeric soft actuator [4]. In this regard, an advance in this field is the use of smart soft-materials for novel wire-less control/actuation through remote stimuli-responsive systems avoiding conventional wire-connections [5,6]. For instance, liquid crystal polymer networks with kirigami designs allowed the design of micro-soft-robots having versatile remote 3D actuation through light-stimulated photomechanical movements [5]. By rolling-up a photomechanical multi-petal structure developed with this smart material, a locomotion was possible through a multiple bending/unbending dynamic using oblique-incidence illumination that allows to the petals push the ground.

From the different strategies for developing smart metamaterials and soft-robots, those based on magnetic actuation are highlighted as magnetic fields are: penetrable, non-destructive, safe, biologically friendly, and fast, without the need of setting any environmental condition [6,7]. Several examples of magnetic smart soft-materials (or magneto-rheological materials) displaying complex shape-morphing and locomotion mechanisms can be found mainly by programing the response through the magnetization/dipole control of the particles embedded into the continuous soft-matrix [8–14]. This strategy allowed for instance millimetric soft-robots with multimodal locomotion under a magnetic field able to swim/climb in liquids, roll/walk/crawl/jump on solid surface, and even perform pick-and-place and payload-release tasks [15]. Despite the outstanding locomotion of these smart materials, they presented limited movement/deformation due to the simple architecture design used, further reducing the possibility of mimic the complex morphology and control of natural locomotion [7]. For instance, an ultra-fast magneto active soft robot having complex geometries can be designed to walk, swim, levitate, transport payload, squeeze into a vessel smaller than their dimensions, and capture a living fly [16]. The use of metamaterial and kirigami structures can further result in a controlled complex shape-morphing behavior programmed by the specific geometry and the response of the magnetic smart-material [7]. By using hinge-linked individual anisotropic blocks with aligned magnetic particles, the kirigami structure can present a set of different 2D and 3D reconfigurable complex shape-motions with fast response [7]. A similar strategy was reported using a 3D printing process coupled with a magnetic field for programming ferromagnetic domains in printed soft-materials that allows 3D complex shape-morphing behaviors under a magnetic field [17]. This strategy was applied to act remotely both an auxetic metamaterial structure (i.e., with negative Poisson-ratio) and a hexapedal structure for wrapping and carrying objects through rolling-based locomotion. Another route used an UV lithography-based method to produce a controlled patterning of magnetic particles in a soft-matrix [18]. By controlling the applied magnetic fields, encoded magnetic polymer sheets with designed-geometries were able to perform multi-axis bending, large-angle bending, and combined bending and torsion shape-morphing, and even a locomotion through a multi-legged paddle crawling.

Complementing the above-mentioned reports designing complex shape-morphing architectures through programmed magnetic alignment under a variety of specific fields, here we introduce a simple smart magnetic auxetic metamaterial based on a kirigami design (rotating-square geometry) that under a magnetic field produced by a commercial magnet, presents multiple locomotion mechanisms. Although there are several kirigami designs for producing magnetic active soft robots, we focused on a rotating-square architecture having an initial (or resting) angle between the squares of zero, by the several advantages that present [19]: 1) easy preparation as it is the simplest cut-design allowing auxetic response (avoiding complex laser-cut equipment); 2) constant Poisson ratio of – 1.0; and 3) in-plane isotropy meaning that the Poisson ratio is the same irrespective of the direction of loading. Moreover, in the resting state does not have free-space maximizing the total force per area exerted by the external magnetic field. In this way, rather than focusing on programming both the magnetization of the particles embedded in the soft-matrix and the shape-morphing responses, we used the "mechanical intelligence" of a highly flexible isotropic magnetic responsive auxetic metamaterial to produce multimodal locomotion. Alongside translational-locomotion, our soft-robot mimics the complex locomotion of crawling limbless animals, such as worms, through a dynamic anchoring process controlling the friction on the surface and moving in a retrograde peristaltic wave. Rolling locomotion can also be performed by our soft robot. All these locomotion processes were obtained without the need of complex shape-morphing behavior or magnetization programs.

2. Materials and methods

Cobalt ferrite ($CoFe_2O_4$) nanoparticles were synthetized using a method similar to that reported by Green et al. [20]. Cobalt Nitrate ($Co(NO_3)_2{\cdot}6H_2O$) (1.8 g, 0.0062 mol) and Iron (II) Chloride ($FeCl_2{\cdot}4H_2O$ (2.4 g, 0.0121 mol) were placed into a 250 mL beaker. Water (100 mL, Millipore) was added and the mixture stirred for an additional 15 min to dissolve the salts. To this was then added a solution of NaOH (10 mL, 3 M) to raise the pH of the solution with an associated color change. This mixture was stirred for an additional 30 min then heated under stirring to below boiling point (80–90°Celsius) for approximately 1 h. The resulting brown/black suspension was isolated using magnetic separation and cleaned repeatedly with water until a neutral pH of the decanted water was achieved then the material was washed twice with ethanol and dried in an oven at 80 °C overnight.

The size and morphology of the synthesized particles were characterized by a scanning electron microscope (FEI QuantaTM 250) equipped with an Octane silicon drift detector for elemental analysis via energy-dispersive X-ray spectroscopy. The magnetization measurements of the magnetic particles were performed by a vibrating sample magnetometer (VSM) at 300 K.

A commercial elastomer (Ecoflex 00–30 from Smooth-On Inc.) was used as the polymer matrix for the preparation of the polymer composite. Part A of Ecoflex was first mixed with the magnetic nanoparticles (26 wt%) through an ultrasound bath (low energy to avoid a cross-linking) for 15 min. Afterward, Part B of Ecoflex (same amount as Part A) was added to the solution and mixed for 10 min in the ultrasound bath. The liquid composite (15 wt%) was added to a mold (made from Ecoflex) and left for at least 60 min for continuing the crosslinking process. The system was then putted in an oven at 60 °C 120 min for finishing the crosslinking process and forming a film of 30 × 30 × 1 mm^3. For the auxetic kirigami design, the pure ecoflex film was cut using a laser cutting equipment (Epilog Legend 360 using air-cooled CO2 laser tubes). For the generation of the magnetic force, a commercial Neodymiun magnet was used consisting in a circular magnet of 35 mm of diameter and 6 mm height.

3. Results and discussion

3.1. Material characterization and smart behavior

The morphology of the synthesized ferrimagnetic cobalt ferrite ($CoFe_2O_4$) nanoparticles is displayed in Fig. 1a while the magnetic response at room temperature as measured by VSM is displayed in Fig. 1b. Nanoparticles having sizes around 30 nm were mainly obtained displaying a ferrimagnetic behavior with a coercivity of 362 (Oe) and a remanent magnetization of 28 (emu/g). These nanoparticles were mixed with the soft-polymer matrix without using any external magnetic field to explore the behavior of an isotropic system rather than a material with aligned nanoparticles and improved dipole-orientation. Fig. 1c shows an optical microscope image of the composite confirming the random/isotropic orientation of the micro-sized agglomerates formed from the nanometric particles. Regarding the tensile behavior, the

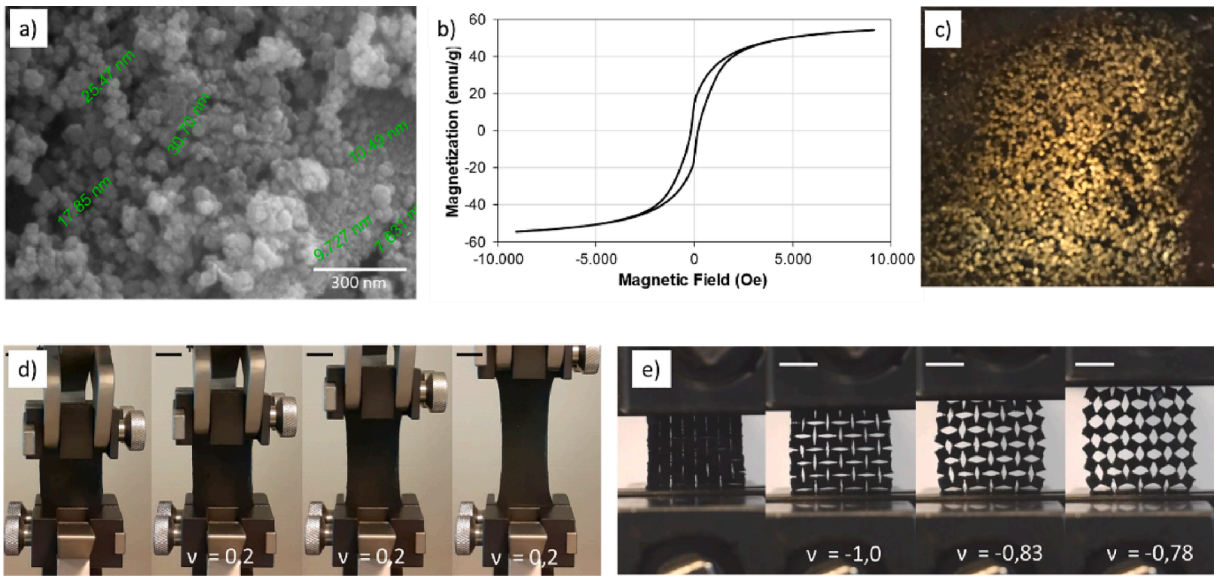

Fig. 1. Main materials characterization and the auxetic behavior of the composites. **A**): Scanning electron microscopy (SEM) image of the synthesized cobalt ferrite ($CoFe_2O_4$) nanoparticles; **B**) vibrating-sample magnetometry (VSM) results from the $CoFe_2O_4$ nanoparticles; **C**) optical microscopy images of the elastomeric composite having embedded $CoFe_2O_4$ nanoparticles; **D**) tensile stress–strain images of the continue elastomer/$CoFe_2O_4$ nanocomposite (ν representing the Poisson ratio); and **E**) tensile stress–strain images of the kirigami auxetic nanocomposite film (ν representing the Poisson ratio). Black-bars in Fig. 1d and white-bars in Fig. 1e represent 20 mm.

resulting continue-film (without the kirigami design) displays the standard elastomeric response (Fig. 1d) meaning a positive Poisson coefficient of 0.2 (i.e. under stretching the film become narrower in the orthogonal axis). An opposite behavior is displayed by the kirigami-film (Fig. 1e) as under stretching the sample become wider (auxetic). At low tensile strains, the sample presents a Poisson ratio of −1.0 that agrees with the theoretical value from a pure rotating-square systems presenting auxetic behavior [19,21]. By increasing the strain, the Poisson ratio change to values around −0.8, meaning that other deformations such as square-stretching and out-of-plane deformation become relevant. Non-perfect squares or imperfections from the laser-cuts can also explain these changes. Noteworthy, the auxetic-kirigami film presented much lower tensile-stiffness than the continue-film with differences around one order of magnitude in the forces needed for strain, for instance 0.53 and 0.02 N for 3 cm deformation, respectively. This flexibility arises from the rotating-squares that are connected at their vertices by hinges, meaning that the stiffness of this auxetic metamaterial depends on the stiffness from the hinges rather than on the elastic modulus of the material [19].

By fixing vertically the samples in the mobile top-section of the tensile-strain equipment and adding a magnet in the fixed bottom-section, the high flexibility of the kirigami sample is confirmed (Fig. 2a-b). While the continue-sample did not deform while moving-closer to the magnet (Fig. 2a), even under contact, the auxetic structure deformed remotely by approaching to the magnet (Fig. 2b), for instance 30% at 0.4 cm with a Poisson ratio of −0.8. By fixing

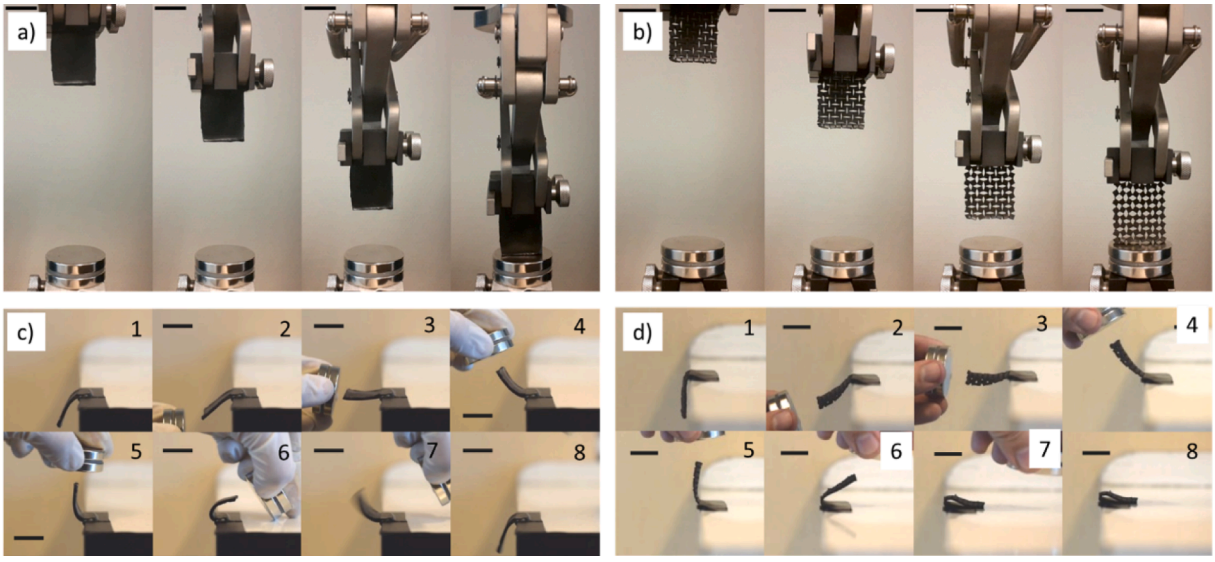

Fig. 2. Comparative images showing the effect of a magnetic field on the behaviour of the continue and kirigami based films. Figures **A** and **B** show the behavior of the continue and kirigami auxetic samples, respectivelly, fixed at the moving top-section of the tensile stress–strain equipement and moving closer to the fixed magnet at the botton-section. Figures **C** and **D** show the behavior of the continue and kirigami auxetic samples, respectivelly, horyzontally fixed at one border under a semicircular-moving magnet closer to the another border.

horizontally one border of the samples, both films response remotely through a vertical bending following the lines of force from the magnet having a semicircular-vertical trajectory close to the another border of the films (Fig. 2c-d). The stiffness of the continue-film produces a null tensile strain-deformation and a reversible behavior after completing a back-forward bending meaning that bending elasticity of the film is higher than the magnetic force in that position (Fig. 2c7). The kirigami-film otherwise strains during the trajectory and stays bended after the cycle due to the out-of-plane rotation of the hinges (Fig. 2d7 and 2d8). These results confirm that the mechanical properties of the kirigami metamaterial are controlled by the pattern of the cuts rather than by the stiffness of the material [22,23].

The driving force for actuation/locomotion in magnetic-active materials is the torque and force generated by the alignment of the ferrimagnetic particles embedded in the soft-matrix with an external magnetic field [6,14]. Magnetoactive materials can respond by simple translation triggered by the attractive force generated by the external magnetic field located in-plane respect to the film with particles having a magnetization alignment in that direction. This translational locomotion was confirmed by putting the samples ($30 \times 30 \times 1$ mm^3) on a smooth-plastic horizontal surface (with a low surface/film friction) and by steadily moving-away in-plane the magnet located under the surface as displayed in Fig. 3a. Both samples were able to follow the magnet by simple translation. This simple translational locomotion appeared when the frictional force generated by the surface on the sample is lower than the force triggered by the magnetic field. By increasing the surface-roughness (for instance by using a sandpaper surface) this translational movement is not observed. This motivated the analysis of more complex locomotive mechanisms such as those find in nature, in particular animal crawling. The ferrimagnetic nanoparticles incorporated into the soft material present a magnetization under a magnetic field without losing this condition when the field is removed (Fig. 1b). The magnet on the other hand presents a non-uniform short-range field with closed-loop lines of force that depending on its relative position respect to the film can produce either attractive or repulsive forces on the magnetized particles. For instance, the particles will have an attractive force when the magnet is located under the film in a N-S direction, but they will have a repulsive force when the magnet is moved next to the film where the lines of forces change of direction relative to the particle-magnetization.

3.2. Biomimetic locomotion

Motivated by the control of the dynamic magnetic force exerted on the particles by changing the relative magnet/particle position, we explored the locomotion of our films using the same set-up but with a magnet having a periodic in-plane movement (Fig. 3b and Supplementary Video 1). The time-varying magnetic field on the sample is obtained by cycles consisting of 3 stages: 1) the center of the circular magnet is located under the head of the film (white lines in Fig. 3b-1); 2) the magnet is in-plane displaced-away (tail to head) to a distance where the lines of force do not reach the sample (Fig. 3b-2); and finally 3) the magnet is in-plane displaced-closer (head to tail) to the sample (Fig. 3b-3) until a position where the center of the magnet matches the new position of the head of the film (Fig. 3b-4). To avoid translational movement, these experiments were carried-out on a surface with a high roughness (sandpaper). The attractive/repulsive oscillating magnetic forces acting on the auxetic matrix, resulted in a complex set of

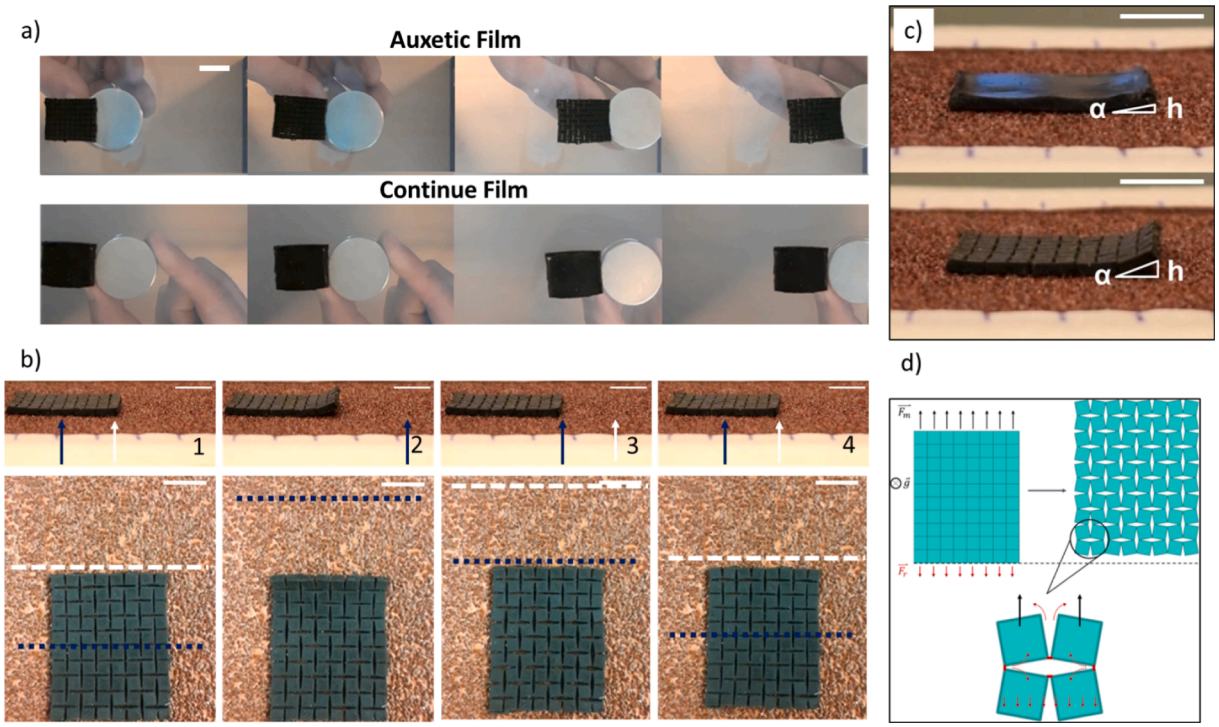

Fig. 3. Locomotion mechanisms. A) Sequence of images of the continue and auxetic films over a smooth plastic surface taken when the magnet (located below the surface) is displaced in-plane from left to right at constant speed, resulting in translational locomotion of the films as the friction force is lower than the attractive magnetic force; **B**) images of the crawling locomotion of the auxetic film over a rough sandpaper surface when the magnet (located below the surface) moved one cycle (white line/arrow represent the position of the center of the magnet while blue line/arrow represent its closest border); **C**) head-lifting of the continue and auxetic films (see Fig. 3b.2) where α represents the angle formed; and **D**) a diagram showing the mechanism for the auxetic deformation (see Fig. 3b.3) due to the attractive forces arising from field-lines getting in the same direction that the magnetization generating a local tensile-strain and a torque on the structure expanding from tail-to-head (F_r and red arrows represent the frictional forces while F_m and black arrows represent the attractive magnetic force where the latter is higher than the former explaining the translational movements). The scale bar represents 5 mm. (For interpretation of the references to color in this figure legend, the reader is referred to the web version of this article.)

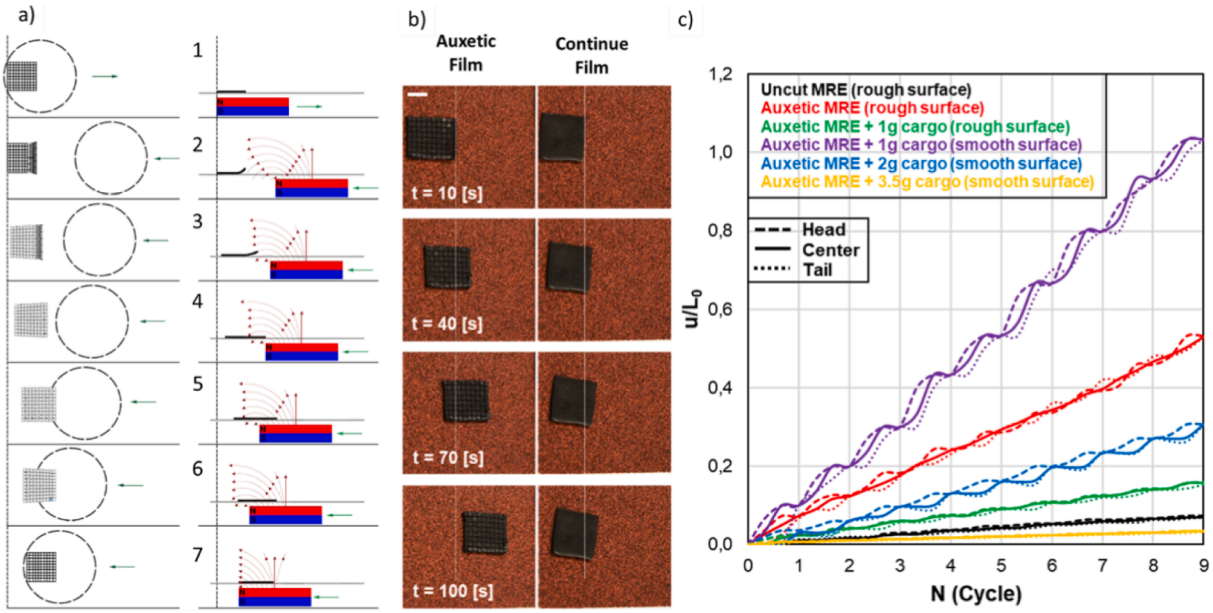

Fig. 4. Auxetic locomotion mechanism of the magnetorheological elastomers (MRE). **A**) Diagram showing the different stages of crawling observed on the kirigami film (black square in the left-side and horizontal black line in the right-side) under one cycle of the magnet (circle in the left-side and red/blue rectangle in the right-side); **B**) crawling locomotion of the continue and auxetic films after several cycles of the periodic magnet movement (vertical while line represent the original position of the head of the films); and **C**) a plot showing the travelled distance (measured from the head, center and tail) as function of the magnet displacement cycles for the continue and kirigami films under different conditions: smooth and roughness surface and during transport of a payload (cargo). L_0 = length of the film and u = displacement. Scale bar in Fig. 4b represents 5 mm. (For interpretation of the references to color in this figure legend, the reader is referred to the web version of this article.)

actuations. This dynamic actuation mimics a crawling-locomotion after one cycle as displayed in Fig. 3b, that is mainly triggered by a head-lifting (Fig. 3b-2 and 3c) and the tensile-strain through the rotation of the squares as observed in Fig. 3b-3 and diagramed in Fig. 3d. Fig. 4a displays a diagram showing the different forces exerted on the auxetic film as a function on the magnet location that explains the crawling locomotion after one cycle. After magnetization in Stage 1 (Figs. 3b-1 and 4a-1) and during Stage 2 and 3, some lines of force from the magnet will present a direction opposite to the sample magnetization and a head-lift process appears due to the repulsive forces (Figs. 3b-2 and 4a-2). As the magnet moves-closer, an attractive force appears on the lifted head-area of the auxetic film due to some field-lines getting in the same direction of the magnetization (Fig. 4a-3). This attractive force generates a local tensile-strain and torque on the lifted auxetic-structure expanding from tail-to-head and producing a translation (Fig. 4a-3). As the magnet moves even further, the attraction affects most of the film, pushing-down the sample in an expanded state (around 8 %) (see Fig. 3b-3 and Fig. 4a-4). Finally, as the magnet continue moving, the auxetic-film relaxes from head to tail, increasing the translation during the process (Figs. 3b-4, 4a-5,6,7) and the friction on the surface. These actuations patterns are barely observed in the continue-film and for instance in the head-lifting process the continue-film presents an angle $\alpha = 11°$ and a vertical displacement of 1.2 mm, while the auxetic-film has values of 22° and 2.3 mm (Fig. 3c). Indeed, after several-cycles of the magnet motion, the displacement of the auxetic-film is much higher than the continue-film (see Fig. 4b), due to the flexibility of the kirigami-film.

To automate the displacement of magnets and to better tune the itinerary of each motion cycle we mounted the magnet on a small linear guide (ball screw) actuated by a stepper motor (Nema 23). The servo motor was connected to a RAMP 1.4 controller mounted over an Arduino Mega board and interfaced to a host computed computer by a serial USB communication. The motion program was considered and the servo locate the magnet under the new position of the film resulting

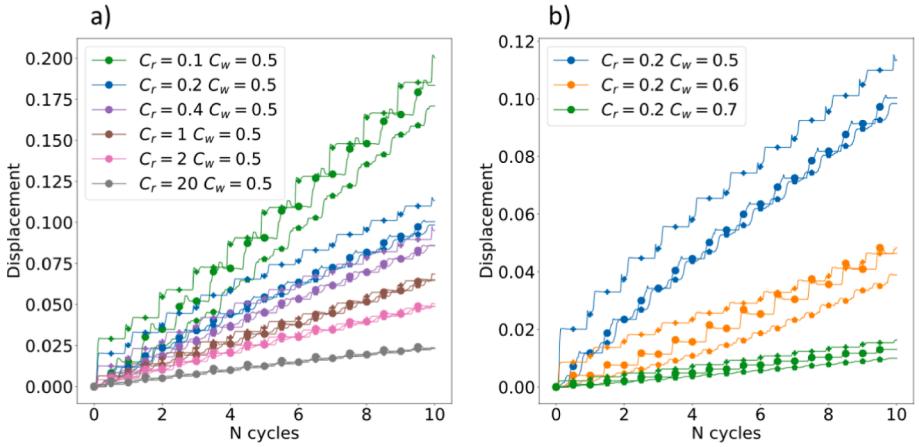

Fig. 5. Theoretical results from the auxetic locomotion mechanism. Effect of the number of magnet cycles on the relative displacement (ratio between the net displacement of the soft robot and its length) from the numerical simulations assuming that the kirigami soft robot is composed by a rectangular array of rotating solid blocks connected at the shared corners through springs: **A**) results from different normalized rotational elastic coefficients (Cr); and **B**) results from different normalized film weights (Cw). The rotational elastic coefficient is normalized by the maximum magnetic torque, and the weight is normalized by the maximum magnetic force. The relative displacement was measured from head (+), middle (o) and tail (*) section of the kirigami soft robot.

from the locomotion in Stage 3. The crawling-speed therefore will depend not only on the characteristic times of the hardware (i.e., stepper motor) but also on the specific displacement program. For instance, the continue-film needs 28 min for advance 10 cm (around 3 times the length of the films) with a program optimized for its displacement, while the auxetic-film needs 21 min under the same program. This means that even under an optimal condition for the continue-film locomotion, the auxetic-film move faster. Noteworthy, for a program designed for the auxetic-film, this time is reduced to only 4 min while the continue-film barely move. In this way, under an optimum controller program for each film the speed is 3.6 mm/min for the continue-film and 25 mm/min for the kirigami-film, confirming the relevance of the flexibility and auxetic-structure for the crawling-locomotion. Fig. 4b displays an example of the different locomotion speed for both samples under the optimum program for each sample, while Fig. 4c shows the relative displacement for each sample depending on the number of cycles. Fig. 4c confirms the much higher speed (around 7 times) of the kirigami-film as compared with the continue-film. Fig. 4c further allows the measurement of the locomotion (or movement) efficiency defined as the ratio of the distance moved per cycle to the maximum dimension of the soft robot, meaning the slope of this figure. This definition allows the comparison with other soft robots as reported previously [24]. The locomotion efficiency in our kirigami soft robot was 6% that although is low as compared with soft robots having other mechanisms (for instance slithering locomotion or sandfish soft robots having efficiencies around 25%), it is in the range of a caterpillar and quadruped soft robots [24].

From the theoretical perspective, a series of simulations were carried out that captured all of the system's basic features. These simulations followed the ideas presented in [25] that allow the formulation of auxetic toy models, that is, minimal models that capture the essential behavior of the auxetic conformations. One such model is a rectangular array of solid blocks that can be displaced and rotated. Such blocks connect at the shared corners through springs that restrict their displacement, torsion, and bending. In tuning the different parameters of the system, we focused on the Poisson ratio, exploring the region of elastic parameters where it was negative. In addition to the springs, respective weights, and frictional forces, we acted on the blocks through magnetic forces and torques acting on each block. Those calculated forces are the magnetic response to the external magnet outside the system. The external magnetic field has the dual role of 1) inducing a net dipolar moment density by orienting the moment of the ferrimagnetic particles embedded in the polymer [26] and 2) exerting forces and torques onto it [27]. The resulting numerically equations of motion were solved with a Runge-Kutta procedure running on GPU [28]. Different simulations with various sources of dissipation (such as viscous drag or Coulomb's frictional) were carried out allowing to confirm that the auxetic oscillatory motion requires static friction (i.e., a much greater frictional force between the material and the surface, as compared with the magnetic pull), as in a system without friction only translational locomotion was observed (as similar as the locomotion observed in Fig. 3a).

The numerical simulations under friction are in startling agreement with the experimental findings as a locomotion process is obtained that mimics the crawling-process (see Supplementary Video 2 for details). This locomotive mode is mediated through the collective auxetic behavior of the underlying geometry of the system that takes hold of the system's motion. The simulated displacement for each cycle is in excellent agreement with the experimental results as concluded comparing Fig. 4c and Fig. 5. Our model further stresses the relevance of the kirigami design through the large effect of the rotational elastic coefficient (Cr) producing a systematic reduction in the locomotive mode (Fig. 5a). By increasing this coefficient, a drastic decrease in the speed (slope between relative displacement and number of cycles) of the soft-robot was observed confirming the need of a rotational flexibility of the rectangular array for a relevant locomotion. Indeed, Fig. 5a shows that the speed ratio between the sample with a high rotational elastic value ($Cr = 20$, meaning a much more rigid rotational system) and the same sample but with a low rotational elastic value ($Cr = 0.1$, meaning a flexible rotational system), is as similar as the experimental ratio speed between the continue film and the kirigami film.

These results show that the combination of a smart auxetic kirigami magnetic film with a proper dynamic force field produces a new crawling locomotion for future design of soft-robots having biomimetic locomotion (see Supplementary Video 1). In nature, crawling limbless animals (e.g., worms, caterpillars, snakes, and snails) are able to move in different environment thanks to peristaltic waves of elongation-contraction along the body [29–31]. These peristaltic waves create zones that increase or reduce the anchoring (i.e., friction) of the body to the substrate. This peristaltic-like locomotion driven by dynamic anchoring is the main mechanism that underlies the mechanical principle of the directional migration of limbless crawlers [4,30]. However, the direction of the peristaltic wave can be anterograde (i.e., starting in the back of the organism, and finishing in the head) or retrograde (i.e. starting in the front of the organism, and finishing in the rear). Animals that use anterograde peristaltic wave, like caterpillars, reduce the friction decreasing the size or the segments under contraction [32], while organisms that uses retrograde peristaltic wave, like worms, reduce the friction elongating the segments under contraction [33]. Therefore, our soft-robot mimics the locomotion of the worms, since the dynamic anchoring with a reduction of friction during contraction, moves in a retrograde peristaltic wave. Noteworthy, the biomimetic worm locomotion from our auxetic-soft-robot, in particular the head-lifting (Fig. 3c and Supplementary Video 3), render a capacity to overcome vertical-obstacles using the same set-up, as displayed in Fig. 6a. In particular, the auxetic-film overcome two consecutive obstacles having each one a height equal to the film thickness. By overcoming each obstacle, the worm based soft-robot is located farther from the magnet and the magnetic force decreased producing lower head-lifting angles and length-expansion. For instance, while the angle and length-expansion are 23° and 32 mm for the sample in the original surface, these values change to $\alpha = 17°$ and 13°, and to 31 and 30.5 mm, respectively, after 1 and 2 obstacles (see Fig. 6b).

In summary, the biomimetic crawling locomotion is the result of the auxetic kirigimi design that not only produces a much lower stiffness optimizing the effect of the magnetic field, but also generates a rotational flexibility. The latter triggers specific mechanical response under the dynamic force fields such as an expansion in the two main planar directions (in-plane isotropy) due to the auxetic behavior as confirmed by our numerical simulations. These responses, arising from the specific magnetic forces generated through the magnet movement, produce the dynamic anchoring process needed for the crawling locomotion. These findings open-up the research toward other kirigami or metamaterial geometries able both to increase the flexibility of the active film and to generate an in-plane expansion in the whole locomotion-plane under the stresses generated by the dynamic magnetic field.

3.3. Transport and rolling behavior

An interesting characteristic desired in magneto active soft robots relates with the capacity to transport a payload [15,16,34]. Our biomimetic smart kirigami metamaterial displayed this characteristic with a speed that depended on the weight of the payload and the roughness of the surface (Fig. 4c and Fig. 7), while the continue film did not transport any payload even on a smooth surface. On a rough surface, the worm-based metamaterial was able to transport a payload having the same weight than the smart film although with a locomotion speed around 70% lower than the pure auxetic film. By doubling the weight of the payload, the film was not able to move with a relevant speed. Noteworthy, our theoretical approach was able to simulate this behavior replacing the external payload by an increase in the weight of the material (Fig. 5b). By increasing 20% the sample weight the speed was reduced around 50%.

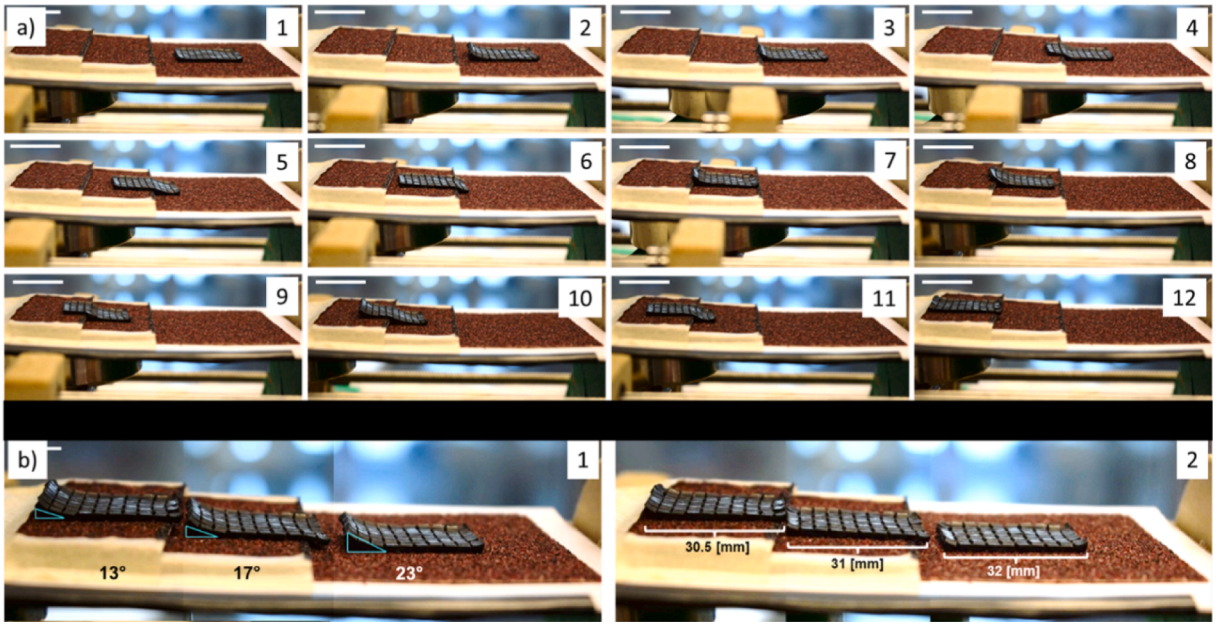

Fig. 6. Auxetic locomotion facing vertical obstacles. **A**) Images from the crawling locomotion of the auxetic films overcoming two vertical obstacles having each one a height of 1 mm (the same that the height of the film) where the numbers represent the time-lapsing; and **B**) images showing the head-lifting angles (left-side) and strained films (right-side) at the original position and after overcoming the obstacles. Scale bar represents 5 mm.

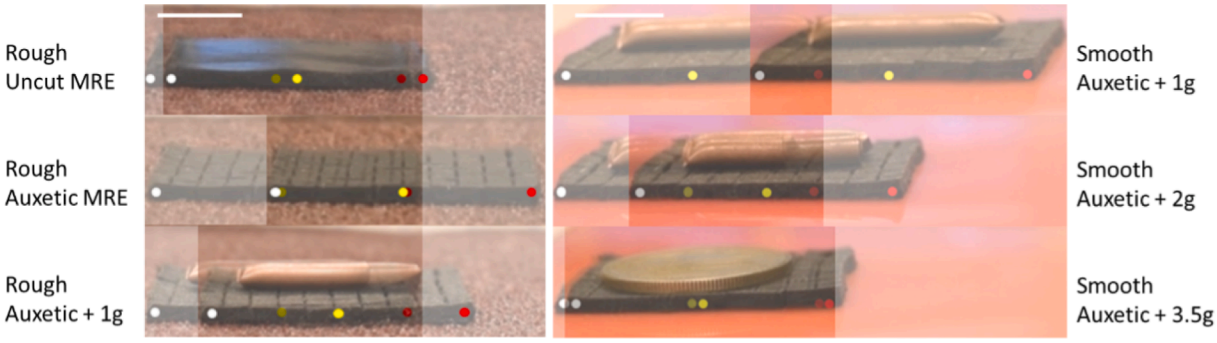

Fig. 7. Locomotion with a payload. Images of the films after one cycle. **Left-side**: continue, auxetic film, and auxetic film with a payload of 1.0 g over a roughness surface; and **Right-side**: auxetic films with payloads having weights of 1.0, 2.0 and 3,5 g over a smooth surface. White, yellow and red points represent left-border, center and right-border of the films respectively, where diffuse-colors and dense-colors represent the original and after one-cycle position of the films. Scale bar represents 5 mm. (For interpretation of the references to color in this figure legend, the reader is referred to the web version of this article.)

By changing the surface from a sandpaper (rough) to a plastic (smooth) surface, the soft robot with the payload having its same weight increased the locomotion speed as compared with the pure soft robot on a rough surface (Fig. 4c and Fig. 7). Noteworthy, on this surface the soft robot was able to transport a payload doubling its weight even with a speed faster than the obtained under a rough surface with a payload having the same weight. By increasing the weight of the payload to 3.5 times the weight of the soft robot, the speed decreased dramatically (Fig. 4c). Fig. 7 displays a summary of the effect of the weight of the payload and the surface on the locomotion of our biomimetic soft robot.

Beside crawling, some soft animals (for instance caterpillars of the family *Crambidae*) presented a rolling locomotion that is an anti-predatory strategy of locomotion based on the capacity of these soft bodies to curl up into a wheel-like structure and rolling downward on a surface thanks to gravity [32,35]. Rolling locomotion can also be found in other animals such as Woodlouse, Namib Golden Wheel Spider, larvae of Lepidopterans, and Stomatopod shrimps, motivating different kind of bioinspired rolling robots [36–38]. For instance, a caterpillar-like robot called GoQBot was developed which closely mimics this rolling strategy [37]. Beside translation and crawling locomotion, our auxetic film further presents a rolling locomotion when the magnet located below the sample is rotated and translated as displayed in Fig. 8a. Under this rotational magnetic field, first the auxetic film rolls on its axe forming a cylinder that afterward move by rolling. The mechanism for our rolling locomotion is displayed in Fig. 8b, based on the torque acting to align the particle magnetization with the field meaning that under a rotating magnetic field the sample will rotate. The rolled kirigami-film can easily roll forward and backward by controlling the rotation direction of the magnet. Therefore, depending on the dynamic of the magnetic field, the smart kirigami films can display translational, crawling, and rolling locomotion mechanisms. Under this magnetic field, the elasticity and higher stiffness of the continue film (as showed comparing Fig. 2c and 2d) did not allow the rolling locomotion showing that the kirigami design facilitates this movement.

4. Conclusions

By designing a smart rotating-square kirigami elastomeric film with embedded random ferrimagnetic nanoparticles, a highly flexible soft robot was developed that can be remotely acted by a simple commercial

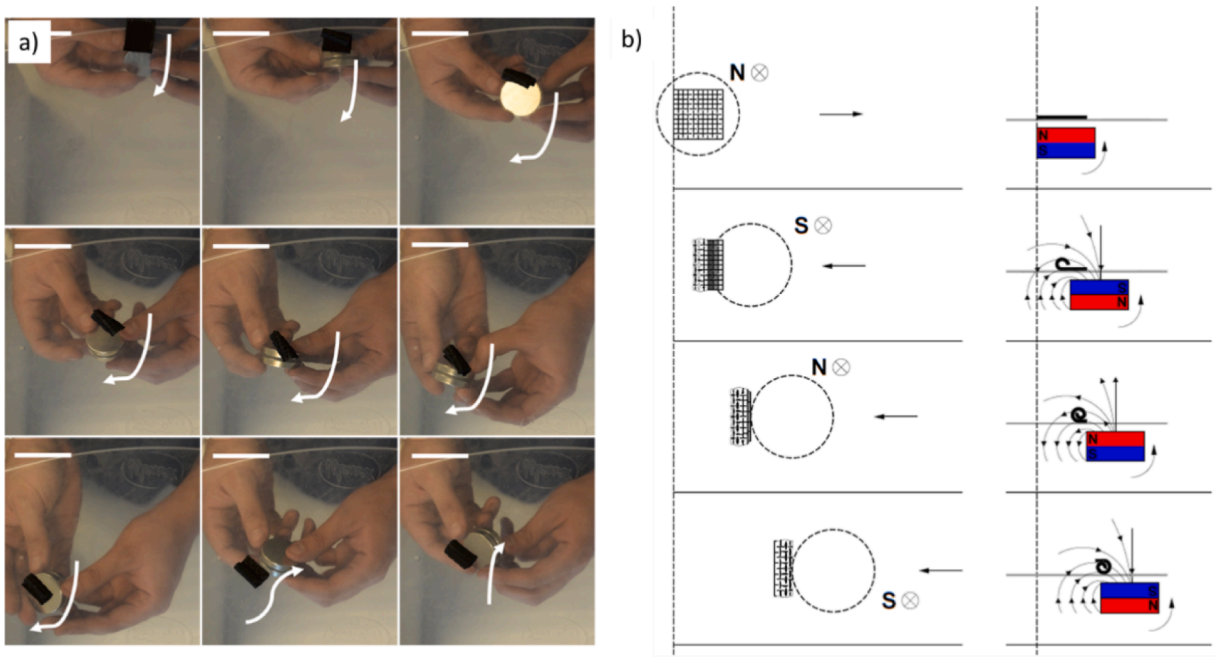

Fig. 8. Rolling auxetic locomotion. **A**) Images from the rolling-locomotion of the kirigami film starting with its rolls on an axe forming a cylinder that afterward is able to move by rolling; and **B**) diagram showing the different stages of the rolling locomotion from the kirigami film (black square in the left-side and horizontal black line in the right-side) under one cycle of the magnet (circle in the left-side and red/blue rectangle in the right-side). Scale bar represents 5 mm. (For interpretation of the references to color in this figure legend, the reader is referred to the web version of this article.)

magnet. The flexibility of the resulting smart auxetic metamaterial soft-robot allowed several locomotion mechanisms alongside the standard translational movement, depending on the magnetic field. For instance, under a horizontal oscillatory magnetic field over a high-roughness surface, the kirigami soft robot mimicked the crawling-locomotion of worms through a dynamic anchoring process, even climbing vertical-obstacles with twofold the height of the film. A theoretical simulation confirmed the relevance of the kirigami design on the locomotion, in particular stressing the need of a high flexible rotational elasticity and the friction. The worm-based locomotion generated under this magnetic field further allowed to the soft-robot transports a payload with a speed depending on the surface roughness and the weight of the cargo. For instance, under a smooth-surface, the soft-robot can transport a payload having the double of its weight. By properly orienting the magnetic field, the smart auxetic structure can further mimic the rolling locomotion of some soft-body animals meaning multiple remote locomotion mechanisms. Our results showed that kirigami based metamaterials having isotropic magnetic properties represent a novel strategy to design flexible smart soft-robots remotely actuated by magnetic forces.

Declaration of Competing Interest

The authors declare that they have no known competing financial interests or personal relationships that could have appeared to influence the work reported in this paper.

Data availability

Data will be made available on request.

Acknowledgements

This work was funded by the projects ANID – Millennium Science Initiative Program – Code NCN17_092, ANID-Basal Center of Interventional Medicine for Precision and Advanced Cellular Therapy, IMPACT, # FB210024, ANID-Fondecyt Regular 1230515, and ANID-Fondecyt Iniciación 11201249.

Appendix A. Supplementary data

Supplementary data to this article can be found online at https://doi.org/10.1016/j.matdes.2023.112262.

References

[1] S. Kim, C. Laschi, B. Trimmer, Soft robotics: a bioinspired evolution in robotics, Trends Biotechnol. 31 (5) (2013) 287–294.
[2] A. Rafsanjani, K. Bertoldi, A.R. Studart, Programming soft robots with flexible mechanical metamaterials, Sci. Rob. 4 (2019) eaav7874.
[3] B. Grossi, H. Palza, J.C. Zagal, C. Falcón, G. During, Metarpillar: Soft robotic locomotion based on buckling-driven elastomeric metamaterials, Mater. Des. 212 (2021), 110285.
[4] A. Rafsanjani, Y. Zhang, B. Liu, S.M. Rubinstein, K. Bertoldi, Kirigami skins make a simple soft actuator crawl, Sci. Rob. 3 (2018) eaar7555.
[5] Y.C. Cheng, H.C. Lu, X. Lee, H. Zeng, A. Priimagi, Kirigami-Based Light-Induced Shape-Morphing and Locomotion, Adv. Mater. 32 (2020) 1906233.
[6] J.G. Kim, J.E. Park, S. Won, J. Jeon, J.J. Wie, Contactless Manipulation of Soft Robots, Materials 12 (2019) 3065.
[7] T. Jiralerspong, G. Bae, J.-H. Lee, S.-K. Kim, Wireless Control of Two- and Three-Dimensional Actuations of Kirigami Patterns Composed of Magnetic-Particles–Polymer Composites, ACS Nano 14 (12) (2020) 17589–17596.
[8] G.Z. Lum, Z. Ye, X. Dong, H. Marvi, O. Erin, W. Hu, M. Sitti, Shape-programmable magnetic soft matter, PNAS 113 (2016) E6007–E6015.
[9] J.E. Park, J. Jeon, J.H. Cho, S. Won, H.J. Jin, K.H. Lee, J.J. Wie, Magnetomotility of untethered helical soft robots, RSC Adv. 9 (2019) 11272.
[10] J. Kim, S.E. Chung, S.E. Choi, H. Lee, J. Kim, S. Kwon, Programming magnetic anisotropy in polymeric microactuators, Nat. Mater. 10 (2011) 747–752.
[11] H. Lu, M. Zhang, Y. Yang, Q. Huang, T. Fukuda, Z. Wang, Y. Shen, A bioinspired multilegged soft millirobot that functions in both dry and wet conditions, Nat. Commun. (2018) 3944.
[12] S. Qia, H. Guo, J. Fua, Y. Xie, M. Zhu, M. Yu, 3D printed shape-programmable magneto-active soft matter for biomimetic applications, Compos. Sci. Technol. 188 (2020), 107973.
[13] S. Won, S. Kim, J.E. Park, J. Jeon, J.J. Wie, On-demand orbital maneuver of multiple soft robots via hierarchical magnetomotility, Nat. Commun. 10 (2019) 4751.
[14] Z. Ren, R. Zhang, R.H. Soon, Z. Liu, W. Hu, P.R. Onck, M. Sit, Soft-bodied adaptive multimodal locomotion strategies influid-filled confined spaces, Sci. Adv. 7 (2021) eabh2022.
[15] W. Hu, G.Z. Lum, M. Mastrangeli, M. Sitti, Small-scale soft-bodied robot with multimodal locomotion, Nature 554 (7690) (2018) 81–85.

[16] X. Wang, G. Mao, J. Ge, M. Drack, G.S.C. Bermúdez, D. Wirthl, R. Illing, T. Kosub, L. Bischoff, C. Wang, J. Fassbender, M. Kaltenbrunner, D. Makarov, Untethered and ultrafast soft-bodied robots, Commun. Mater. 1 (2020) 67.
[17] Y. Kim, H. Yuk, R. Zhao, S.A. Chester, X. Zhao, Printing ferromagnetic domains for untethered fast-transforming soft materials, Nature 558 (7709) (2018) 274–279.
[18] T. Xu, J. Zhang, M. Salehizadeh, O. Onaizah, E. Diller, Millimeter-scale flexible robots with programmable three-dimensional magnetization and motions, Sci. Rob. 4 (2019) eaav4494.
[19] J.N. Grima, K.E. Evans, Auxetic behavior from rotating squares, J. Mater. Sci. Lett. 19 (2000) 1563–1565.
[20] D. Greene, R. Serrano-Garcia, J. Govan, Y.K. Gun'ko, Synthesis Characterization and Photocatalytic Studies of Cobalt Ferrite-Silica-Titania Nanocomposites, Nanomaterials 4 (2014) 331–343.
[21] D. Attard, E. Manicaro, R. Gatt, J.N. Grima, On the properties of auxetic rotating stretching squares, Physica Status Solidi (b) 246 (9) (2009) 2045–2054.
[22] D.G. Hwang, M.D. Bartlett, Tunable Mechanical Metamaterials through Hybrid Kirigami Structures, Sci. Rep. 8 (2018) 3378.
[23] T.C. Shyu, P.F. Damasceno, P.M. Dodd, A. Lamoureux, L. Xu, M. Shlian, M. Shtein, S.C. Glotzer, N.A. Kotov, A kirigami approach to engineering elasticity in nanocomposites through patterned defects, Nat. Mater. 14 (8) (2015) 785–789.
[24] Y. Cao, Y. Liu, Y. Chen, L. Zhu, Y. Yan, X. Chen, A novel slithering locomotion mechanism for a snake-like soft robot, J. Mech. Phys. Solids 99 (2017) 304–320.
[25] D. Acuna, F. Gutiérrez, R. Silva, H. Palza, A.S. Nunez, G. Düring, A three step recipe for designing auxetic materials on demand, Commun. Phys. 5 (1) (2022) 1–9.
[26] D. C. Jiles, Introduction to Magnetism and Magnetic Materials (2 ed.), CRC. p. 3. ISBN 978-0412798603. 1998.
[27] D.J. Griffiths, Introduction to Electrodynamics, (4th ed.)., Cambridge University Press, 2017. ISBN 9781108357142.
[28] NVIDIA, Vingelmann, P., & Fitzek, F. H. P. CUDA, release: 11.7.1. Retrieved from https://developer.nvidia.com/cuda-toolkit 2022.
[29] R.M. Alexander, Principles of animal locomotion, Princeton University Press, 2013.
[30] Y. Tanaka, K. Ito, T. Nakagaki, R. Kobayashi, Mechanics of peristaltic locomotion and role of anchoring, J. R. Soc. Interface 9 (67) (2012) 222–233.
[31] D. Agostinelli, F. Alouges, A. DeSimone, Peristaltic waves as optimal gaits in metameric bio-inspired robots, Front. Rob. AI 5 (2018) 99.
[32] J. Brackenbury, Fast locomotion in caterpillars, J. Insect Physiol. 45 (6) (1999) 525–533.
[33] H. Fang, Y. Zhang, K.W. Wang, Origami-based earthworm-like locomotion robots, Bioinspir. Biomim. 12 (2017), 065003.
[34] S.R. Goudu, I.C. Yasa, X. Hu, H. Ceylan, W. Hu, M. Sitt, Biodegradable Untethered Magnetic Hydrogel Milli-Grippers, Adv. Funct. Mater. 30 (2020) 2004975.
[35] J. Brackenbury, Caterpillar kinematics, Nature 390 (6659) (1997) 453.
[36] X. Wei, Y. Tian, S. Wen, Design and locomotion analysis of a novel modular rolling robot, Mech. Mach. Theory 133 (2019) 23–43.
[37] H.T. Lin, G.G. Leisk, B. Trimmer, GoQBot: a caterpillar-inspired soft-bodied rolling robot, Bioinspir. Biomim. 6 (2011), 026007.
[38] M.T. Hou, H.M. Shen, G.L. Jiang, C.N. Lu, I.J. Hsu, J.A. Yeh, A rolling locomotion method for untethered magnetic microrobots, Appl. Phys. Lett. 96 (2010), 024102.